

Magnetic Field Effects and Transverse Ratchets in Charge Lattices Coupled to Asymmetric Substrates

C. J. O. Reichhardt and C. Reichhardt

Theoretical Division and Center for Nonlinear Studies, Los Alamos National Laboratory, Los Alamos, New Mexico 87545, USA

E-mail: cjrx@lanl.gov

Abstract. We examine a charge lattice coupled to a one-dimensional asymmetric potential in the presence of an applied magnetic field, which induces gyrotropic effects in the charge motion. This system could be realized for Wigner crystals in nanostructured samples, dusty plasmas, or other classical charge-ordered states where gyrotropic motion and damping can arise. For zero magnetic field, an applied external ac drive can produce a ratchet effect in which the particles move along the easy flow direction of the substrate asymmetry. The zero field ratchet effect can only occur when the ac drive is aligned with the substrate asymmetry direction; however, when a magnetic field is added, the gyrotropic forces generate a Hall effect that leads to a variety of new behaviors, including a transverse ratchet motion that occurs when the ac drive is perpendicular to the substrate asymmetry direction. We show that this system exhibits commensuration effects as well as reversals in the ratchet effect and the Hall angle of the motion. The magnetic field also produces a nonmonotonic ratchet efficiency when the particles become localized at high fields.

1. Introduction

When overdamped particles are coupled to an asymmetric substrate, a ratchet effect can occur when an ac drive is applied, leading to a net dc transport in the direction of the substrate asymmetry. Ratchet effects have been studied for various systems in the single particle limit [1, 2, 3], including colloidal systems [4, 5], biological systems [6], active matter [7], granular matter [8], cold atoms [9, 10], superconducting vortices [11, 12] and quantum systems [13]. For a single overdamped particle, the ratchet effect produces directed motion in the easy direction of the substrate asymmetry. When collective interactions become important, new behaviors emerge, including commensuration effects that appear when the spacing between the particles matches the substrate length scale. As a result, peaks or dips appear in the ratchet efficiency, as observed in interacting disk systems [14], active matter systems [15] and superconducting vortices [16, 17, 18, 19, 20, 21, 22, 23, 24, 25, 26, 27]. Collective effects can also produce ratchet reversals in which the net dc flux is in the hard direction of the substrate asymmetry [16, 17, 18, 19, 15]. In many of these systems, the interactions are short-range; however, collective ratchet effects can also occur in systems with longer-range interactions where the particles would naturally form a triangular lattice in the absence of a substrate, such as vortices in type-II superconductors [16, 19] or magnetic colloids [28]. Ratchet effects can also appear in charged lattices, which arise in solid-state systems including Wigner crystals [29, 30, 31, 32], charged colloids with weak screening [33], optically trapped ions [34], and dusty plasmas [35].

Charged systems form crystalline states when the Coulomb energy dominates over the thermal or kinetic energy, and they can exhibit ratchet effects when coupled to an asymmetric substrate [35, 36]. Little is known, however, about how the ratchet effect is modified when a magnetic field is applied that causes the moving charges to undergo cyclotron-like displacements [37, 38]. Previous work on so-called electron pinball states showed that cyclotron motion can strongly influence the transport of charged systems coupled to a periodic substrate, resulting in electron localization when the cyclotron orbits become commensurate with the periodicity of the substrate or permitting delocalized and chaotic motion for incommensurate orbits [39, 40]. When a dc drive is applied in addition to the magnetic field, the particles move with a finite Hall angle, and in the presence of a two-dimensional (2D) periodic substrate, the motion becomes locked to specific symmetry directions of the substrate, producing a quantization of the Hall angle as a function of the magnetic field [41, 42]. Recently, it was shown that when a Wigner crystal in a magnetic field is driven over random disorder, the sliding dynamics occur at a finite Hall angle that is drive dependent since the charges are more strongly scattered by the disorder at low drives [43].

For particles coupled to one-dimensional (1D) asymmetric substrates, a ratchet effect only occurs when the ac drive is applied parallel to the substrate asymmetry direction; however, once a Hall effect and cyclotron motion are introduced, it should be possible for a ratchet effect to appear even for ac drives applied perpendicular to the substrate asymmetry direction, with the ratcheting motion consisting of a combination of motion parallel and perpendicular to the drive. In magnetic skyrmions, where the Magnus force can have a strong impact [44, 45] and can cause the skyrmion motion to obey the same dynamics as charges in magnetic fields [46, 44], there have been several studies showing that new kinds of gyrotropic-induced ratchet effects arise [25, 47, 48, 49]. A transverse skyrmion ratchet was also observed in which the ac driving can be applied at any angle with respect to the substrate asymmetry direction [50, 47]. Since the chiral motion itself breaks a symmetry, ratchet effects in skyrmion systems can even occur when the substrate is symmetric [51]. Ratchet effects have been found in other systems with chiral motion, even when the substrates

are symmetric [52, 53, 35]. This suggests that similar gyrotropic ratchet effects can arise in non-skyrmion systems of charged particles in a magnetic field.

Of the numerous classical charged systems that form lattice states due to Coulomb interactions, the best known is Wigner crystals of 2D electrons at low densities [29, 31, 32], which can form in elections on liquid helium [54, 55] or in solid-state systems [56, 57, 58, 59, 60, 61, 62, 63, 30, 64, 65]. There have been several studies of 2D Wigner crystals coupled to 1D or quasi-1D nanostructured channels or arrays [66, 67, 68, 69, 70, 71], while more recently, Wigner crystals coupled to 2D periodic substrates have been studied in moiré heterostructures [72, 73, 74, 75, 76, 77, 78] and dichalcogenide monolayers [79]. Under an applied driving force, Wigner crystals can exhibit sliding states and nonlinear transport [59, 60, 61, 62, 80, 81, 63, 82, 64, 65, 49]. There have also been studies examining diode [83] and ratchet effects [36] for Wigner crystals coupled to asymmetric substrates in the absence of a magnetic field. Other charged systems that could be coupled to asymmetric substrates include dusty plasmas [84, 35] and ion crystals [34]. Point vortices in fluids with long-range interactions are undamped but otherwise similar to charges in a magnetic field, and under circumstances where damping is present in the fluid, the point vortices also exhibit a finite Hall angle under an applied drift force [85].

Previous work on skyrmions interacting with an asymmetric 1D substrate focused only on the single skyrmion limit [25], so collective effects on the motion of gyrotropic particles over an asymmetric substrate have not yet been addressed. Additionally, the interactions for skyrmions generally involve either short-range or intermediate repulsion. Open questions include how a strongly interacting system with gyrotropic dynamics would behave on an asymmetric substrate, and what impact collective effects would have on the behavior.

Here, we consider a 2D assembly of charged particles in the presence of an asymmetric 1D substrate under an ac drive applied either parallel or perpendicular to the substrate asymmetry direction. We specifically study the effect of an applied magnetic field, which creates velocity components that are perpendicular to the net force experienced by a charged particle. When the magnetic field is zero, a ratchet effect occurs only when the ac drive is applied parallel to the substrate asymmetry direction, as found in previous work [36]. For finite magnetic fields, we find that ratchet effects can occur when the ac driving is either parallel or perpendicular to the substrate asymmetry direction. In general, the direction of motion is at an angle with respect to the direction of the ac drive. The efficiency of the transverse and other magnetic ratchet effects is generally non-monotonic as a function of field since the moving charges become localized at higher fields and execute small cyclotron orbits that remain confined within a single pinning trough. We also observe commensuration effects that arise when the cyclotron orbit radius matches the substrate periodicity, as well as a number of ratchet reversals that produce a reversal in the Hall angle. In addition to providing examples of new types of ratchet effects, our results suggest that a transverse ratchet may be used to detect the presence of Wigner crystals in a magnetic field.

2. Simulation

We consider a two-dimensional system with periodic boundary conditions in the x and y directions containing N_e particles with repulsive Coulomb interactions. The particles also interact with a one-dimensional asymmetric substrate. The sample is of size $L \times L$ with $L = 36$ and the particle

density is $\rho = N_e/L^2$. The overdamped equation of motion for charge i is given by

$$\alpha_d \mathbf{v}_i = \sum_j^{N_e} \nabla U(r_{ij}) + q\mathbf{B} \times \mathbf{v}_i + \mathbf{F}_{\text{sub}} + \mathbf{F}_{AC} + \mathbf{F}^T. \quad (1)$$

Here α_d is the damping constant, the particle-particle interaction potential is $U(r_{ij}) = q/r_{ij}$, \mathbf{r}_i and \mathbf{r}_j are the positions of particles i and j , respectively, $r_{ij} = |\mathbf{r}_i - \mathbf{r}_j|$ is the distance between particles, and q is the particle charge which we set to unity. For computational efficiency, we employ a Lekner method for calculating the long-range Coulomb interactions, as used in previous work on charged particles interacting with a substrate [86, 87, 81]. The second term on the right hand side of Eq. (1) describes the Magnus force produced by a finite magnetic field $\mathbf{B} = B\hat{\mathbf{z}}$ applied perpendicular to our 2D sample.

The substrate force $\mathbf{F}_{\text{sub}} = \nabla U(x_i)$ is determined by the x coordinate of particle i , where the substrate potential $U(x)$ has the form

$$U(x) = -U_0[\sin(2\pi x/a) + 0.25 \sin(4\pi x/a)]. \quad (2)$$

This potential produces an asymmetric force profile with a larger force in the negative x -direction. We measure forces in terms of the parameter $A_p = U_0/2\pi$, and we obtain a maximum force in the hard or negative x direction of $F_p^{\text{hard}} = 1.5A_p$ and a maximum force in the easy or positive x direction of $F_p^{\text{easy}} = 0.75A_p$. We have previously used this potential to study Wigner crystal ratchet effects in the absence of a magnetic field [36]. We concentrate on a system size of $L = 36$ with a substrate lattice spacing of $a = 2.117$.

The ac driving force has the form $\mathbf{F}_{AC} = F_{AC} \sin(\omega t)\hat{\alpha}$, where F_{AC} is the amplitude and $\alpha = x$ or y for driving parallel or perpendicular to the substrate asymmetry direction, respectively. We use a time step of $dt = 0.005$ and set $\omega = 0.0000754$, so our typical ac drive cycle spans 10^5 simulation time steps. If we decrease ω to a lower frequency we find no changes in the behavior; thus, our results are of relevance to the low frequency limit. In Section 5 we consider the effects of thermal fluctuations by including the term \mathbf{F}^T , which represents Langevin kicks with the properties $\langle \mathbf{F}_i^T \rangle = 0$ and $\langle \mathbf{F}_i^T(t) \cdot \mathbf{F}_j^T(t') \rangle = 4\alpha_d k_B T \delta_{ij} \delta(t - t')$.

We measure the average velocity per charge in the x and y directions, $\langle V_x \rangle = N_e^{-1} \sum_i^{N_e} \langle \mathbf{v}_i \cdot \hat{\mathbf{x}} \rangle$ and $\langle V_y \rangle = N_e^{-1} \sum_i^{N_e} \langle \mathbf{v}_i \cdot \hat{\mathbf{y}} \rangle$, where the time average is taken over 50 ac drive cycles. We also measure $|\langle V \rangle| = \sqrt{\langle V_x \rangle^2 + \langle V_y \rangle^2}$. When $B \neq 0$ and a magnetic field is present, the charges move at a Hall angle with respect to the drive, which we measure according to $\theta_H = \arctan(\langle V_y \rangle / \langle V_x \rangle)$. The system also has an intrinsic Hall angle, given by $\theta_H^{\text{int}} = \arctan(qB/\alpha_d)$, which increases with increasing B . Interactions with the substrate can cause θ_H to be different from θ_H^{int} , as shown in previous work [43]. Wiersig *et al.* [41] considered charges moving over a 2D periodic array of obstacles under applied magnetic fields that would produce intrinsic Hall angles as large as $\theta_H^{\text{int}} = 60^\circ$. In Fig. 1(a), we show an image of the system with arrows indicating the ac driving direction that is either parallel to the substrate asymmetry direction, giving a longitudinal ratchet effect, or perpendicular to the substrate asymmetry direction, giving a transverse ratchet effect. Figure 1(b) shows a detail of the substrate potential $U(x)$ for a sample where the substrate lattice period is $a = 1$.

3. Results

In Fig. 2(a) we plot $\langle V_x \rangle$ and $\langle V_y \rangle$ versus qB/α_d for a system with $\rho = 0.208$, $A_p = 0.75$, and $F_{AC} = 1.0$. Here, the ac drive is applied along x , parallel to the substrate asymmetry direction. For

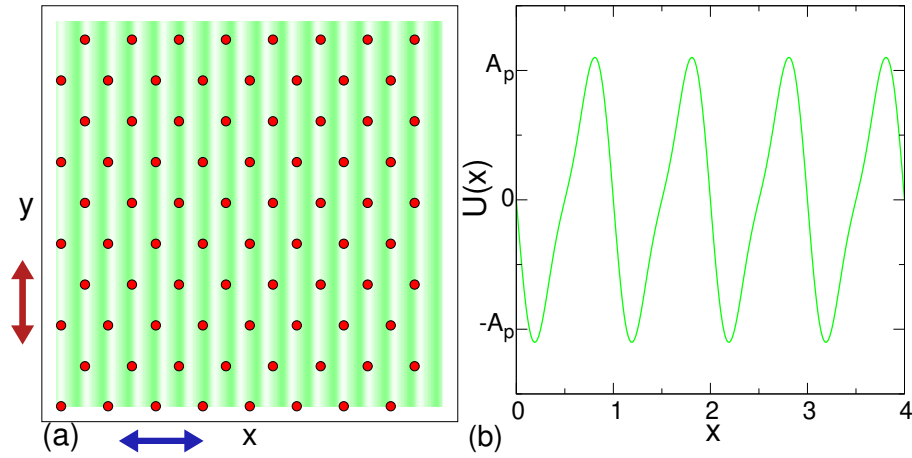


Figure 1. (a) Image of the simulated 2D assembly of charged particles (red circles) interacting with an asymmetric 1D substrate (green shading). An ac drive is applied along the x direction (blue arrow), parallel to the substrate asymmetry direction, or along the y direction (red arrow), perpendicular to the substrate asymmetry direction. (b) Detail of the substrate potential $U(x)$ for a lattice constant of $a = 1$.

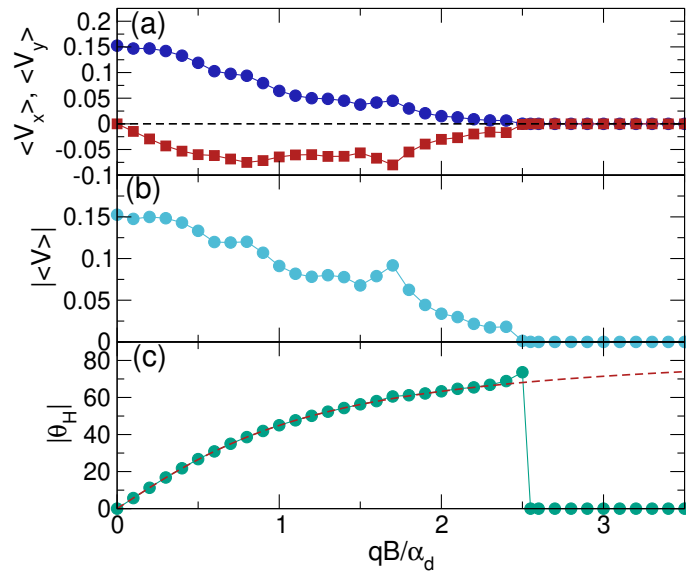


Figure 2. (a) $\langle V_x \rangle$ (blue) and $\langle V_y \rangle$ (red) vs qB/α_d for a system with $\rho = 0.208$, $A_p = 0.75$, and $F_{AC} = 1.0$, where the ac drive is applied along x , parallel to the substrate asymmetry direction. (b) The corresponding $|\langle V \rangle|$ vs qB/α_d . (c) The measured Hall angle $|\theta^H|$ vs qB/α_d . The dashed line is a fit to $\theta^H = \arctan(qB/\alpha_d)$.

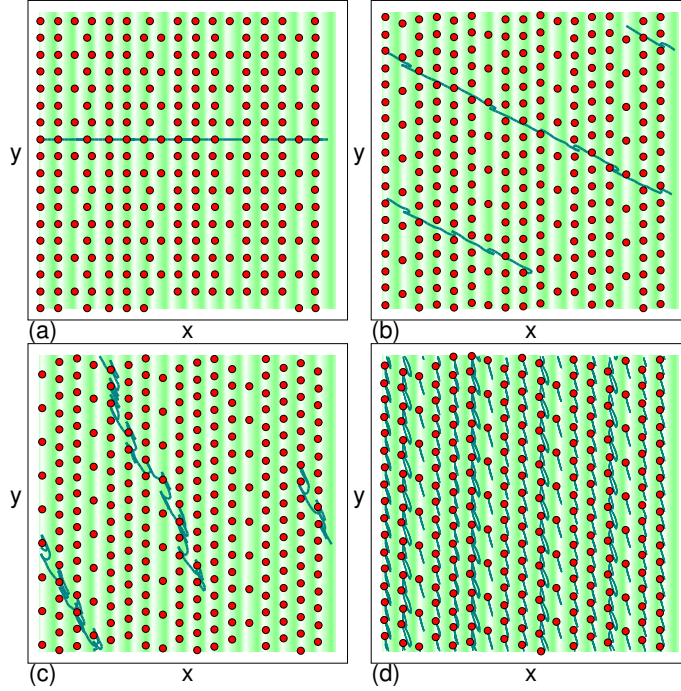


Figure 3. (a,b,c) Particle locations (red circles), substrate (green shading), and the trajectory of a single representative particle (line) for the system in Fig. 2 with $\rho = 0.208$, $A_p = 0.75$, and $F_{AC} = 1.0$ for driving along x , parallel to the substrate asymmetry direction. (a) $qB/\alpha_d = 0.0$. (b) $qB/\alpha_d = 0.5$. (c) $qB/\alpha_d = 2.0$. (d) Trajectories of all particles for $qB/\alpha_d = 3.5$, where the motion is localized and there is no ratchet effect.

this system, the maximum substrate forces are $F_p^{\text{hard}} = 1.125$ and $F_p^{\text{easy}} = 0.5625$. When $B = 0.0$, we find a pronounced longitudinal ratchet effect with $\langle V_x \rangle \neq 0$, as studied in previous work [36]. Figure 2(b) shows the average velocity $|\langle V \rangle|$ versus qB/α_d for the same sample. In Fig. 3(a), we illustrate the particle locations and substrate along with the trajectory of a representative particle during 10 ac drive cycles. The same type of trajectory is followed by all of the other particles, each of which moves only along the x -direction over time with a net motion occurring in the $+x$ direction. In Fig. 2(c), we plot $|\theta_H|$, the absolute value of the measured Hall angle, versus qB/α_d . As B increases, $\langle V_y \rangle$ becomes nonzero when the particles begin to move along the negative y -direction, and a finite Hall angle emerges. With a further increase of B , $|\langle V_y \rangle|$ reaches its maximum value near $qB/\alpha_d = 0.8$ and then diminishes again. The overall velocity $|\langle V \rangle|$ generally decreases with increasing B . For $qB/\alpha_d = 0.5$, the particles move close to an angle of $\theta_H = 30^\circ$, as illustrated in Fig. 3(b), while at $qB/\alpha_d = 2.0$, Fig. 3(c) shows that the particles move along 62° since the Hall angle increases with increasing B . The dashed line in Fig. 2(c) indicates what the Hall angle would be if $A_p = 0.0$, as determined by the expression $\theta_H = \arctan(qB/\alpha_d)$. Near $qB/\alpha_d = 1.7$, we find a local peak in the velocities, corresponding to the field at which the orbit size partially matches the periodicity of the substrate. For $qB/\alpha_d \geq 2.5$, the drift velocities drop to zero because the particle motion becomes localized, as illustrated in Fig. 3(d) where we highlight the trajectories of all of the

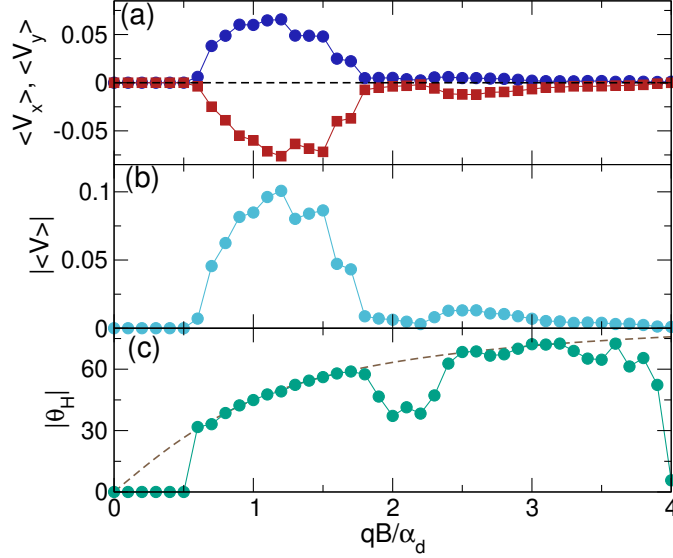


Figure 4. $\langle V_x \rangle$ (blue) and $\langle V_y \rangle$ (red) vs qB/α_d for the system from Fig. 2 with $\rho = 0.208$, $A_p = 0.75$, and $F_{AC} = 1.0$ but with the ac drive applied along the y -direction, perpendicular to the substrate asymmetry direction. (b) The corresponding $|\langle V \rangle|$ vs qB/α_d . (c) $|\theta_H|$ vs qB/α_d . The dashed line is a fit to $\theta_H = \arctan(qB/\alpha_d)$.

particles. For larger B , the particle orbits become more compact and remain confined in a single pinning trough.

In Fig. 4 we plot $\langle V_x \rangle$ and $\langle V_y \rangle$ versus qB/α_d for the same system as in Fig. 2 but with the ac drive applied perpendicular to the substrate asymmetry direction. For $qB/\alpha_d < 0.6$, there is no ratchet effect and both $\langle V_x \rangle$ and $\langle V_y \rangle$ are zero. Figure 5(a) shows the trajectory of a single particle at $qB/\alpha_d = 0.5$, where the particles only move along the y direction and remain localized. There is a large transverse ratchet effect for $0.6 \leq qB/\alpha_d < 1.9$, a reduced ratchet effect appears for $1.9 \leq qB/\alpha_d < 3.9$, and for $qB/\alpha_d \geq 3.9$, the motion is localized again. In Fig. 5(b) at $qB/\alpha_d = 1.2$, the orbit of a single particle consists of a combination of sliding motion along y and jumps along x , giving a net motion that is in the positive x and negative y direction. For $1.9 \leq qB/\alpha_d < 3.9$, the motion is much more chaotic and produces a gradual drift, as illustrated in Fig. 5(c) at $qB/\alpha_d = 2.5$. Figure 5(d) shows that at $qB/\alpha_d = 4.0$, the motion has become localized within the pinning troughs. In Fig. 4(c) we plot $|\theta_H|$ versus qB/α_d along with a dashed line that indicates the behavior expected in a substrate-free system. A dip appears when $1.9 < qB/\alpha_d < 2.5$, where the motion is primarily chaotic with a reduced velocity, as is also visible in the plot of $|\langle V \rangle|$ versus qB/α_d in Fig. 4(b). Our results demonstrate that a magnetic field can induce a ratchet effect even when the ac drive is applied perpendicular to the substrate asymmetry direction, and that this ratchet effect is non-monotonic as a function of the field. The maximum net velocity for the transverse ratchet is close to that of the longitudinal ratchet found for ac driving applied parallel to the substrate asymmetry direction. We find that there is a critical field that must be applied in order for the traverse ratchet to occur, and that the value of this field depends on the strength of the substrate.

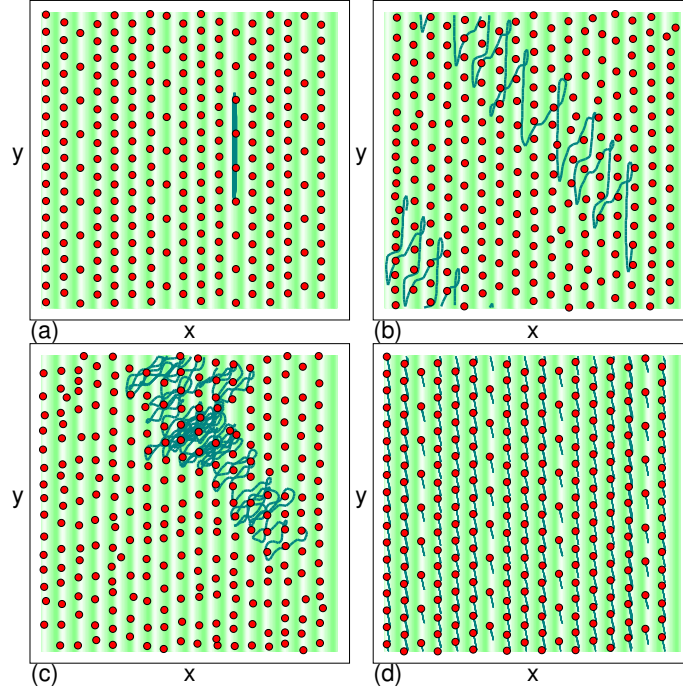


Figure 5. (a,b,c) Particle locations (red circles), substrate (green shading), and the trajectory of a single representative particle (line) for the system in Fig. 2 with $\rho = 0.208$, $A_p = 0.75$, and $F_{AC} = 1.0$ for driving along y , perpendicular to the substrate symmetry direction. (a) $qB/\alpha_d = 0.5$ where the motion consists of oscillations along y . (b) $qB/\alpha_d = 1.2$, showing a 2D periodic translating orbit. (c) $qB/\alpha_d = 2.5$, where the motion is more disordered or chaotic. (d) The trajectories for all the particles at $qB/\alpha_d = 4.0$, where the motion is localized.

In Fig. 6(a), we plot $\langle V_x \rangle$ and $\langle V_y \rangle$ versus A_p for the same system from Fig. 2 with $F_{AC} = 1.0$ and $qB/\alpha_d = 1.2$ under driving perpendicular to the substrate asymmetry direction. Figure 6(b) and (c) show the corresponding $|\langle V \rangle|$ and $|\theta_H|$ versus A_p . There is no ratchet effect at low A_p since the system forms a lattice that effectively floats above the substrate. We find several regions where the ratchet effect goes to zero because the particle orbits become localized. For $A_p > 1.5$, the system is pinned. In Fig. 6(c), the Hall angle in the ratcheting regimes is close to the value expected for a pin-free system. Figure 6(d,e,f) shows $\langle V_x \rangle$, $\langle V_y \rangle$, $|\langle V \rangle|$, and $|\theta_H|$ versus A_p for the same system but for ac driving parallel to the substrate asymmetry direction. Here the ratchet effect is lost for both low and high A_p values.

In Fig. 7(b), we plot time series of the instantaneous values of V_x and V_y (red) for the system in Fig. 2 at $qB/\alpha_d = 0.4$ for ac driving applied parallel to the substrate asymmetry direction, where we find velocity spikes in the positive x direction and smaller spikes in the negative y direction. The additional features in the time series correspond to particle configurations that form during specific portions of the ac drive cycle, since the overall structure of the particles can change as the ac drive direction varies throughout the cycle. At $qB/\alpha_d = 0.0$, Fig. 7(a) shows that spikes are still present in V_x but are absent for V_y . In Fig. 8, we plot the instantaneous V_x and V_y versus time for

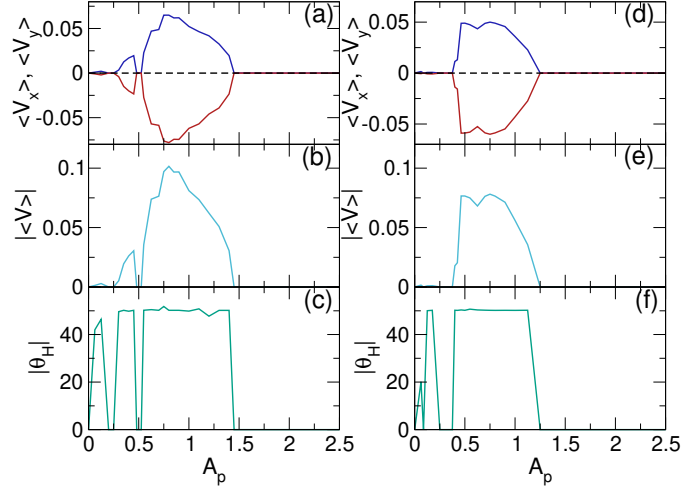


Figure 6. (a) $\langle V_x \rangle$ (blue) and $\langle V_y \rangle$ (red) vs A_p for the system in Fig. 2 with $\rho = 0.208$ and $F_{AC} = 1.0$ at $qB/\alpha_d = 1.2$ for ac driving applied along y direction, perpendicular to the substrate asymmetry direction. (b) The corresponding $|\langle V \rangle|$ vs A_p . (c) The corresponding $|\theta_H|$ vs A_p . (d) $\langle V_x \rangle$ (blue) and $\langle V_y \rangle$ (red) vs A_p for the same system with ac driving applied along x , parallel to the substrate asymmetry direction. (e) The corresponding $|\langle V \rangle|$ vs A_p . (f) The corresponding $|\theta_H|$ vs A_p .

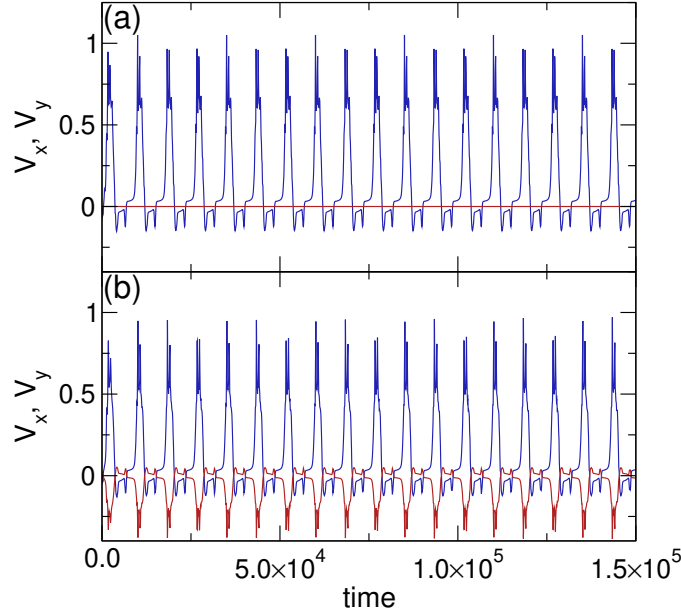


Figure 7. Time series of instantaneous velocities V_x (blue) and V_y (red) for the system in Fig. 2 with $\rho = 0.208$, $A_p = 0.75$, and $F_{AC} = 1.0$ for driving along x , parallel to the substrate asymmetry direction. (a) $qB/\alpha_d = 0.0$, where there is ratcheting motion in the positive x direction but no motion in the y direction. (b) $qB/\alpha_d = 0.4$, where there is a strong ratcheting motion in the x -direction and a smaller ratcheting motion in the negative y -direction.

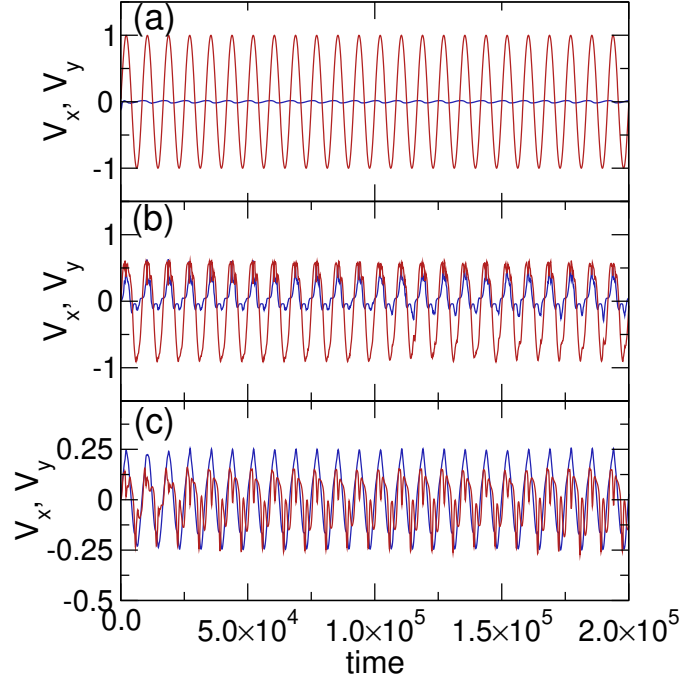


Figure 8. Time series of instantaneous velocities V_x (blue) and V_y (red) for the system in Fig. 2 with $\rho = 0.208$, $A_p = 0.75$, and $F_{AC} = 1.0$ for driving along y , perpendicular to the substrate asymmetry direction. (a) At $qB/\alpha_d = 0.4$, there is no ratcheting motion in either direction. (b) At $qB/\alpha_d = 1.2$, there is ratcheting motion in the positive x -direction and the negative y -direction. (c) At $qB/\alpha_d = 4.0$, there is no ratcheting motion in either direction.

the same system with ac driving applied perpendicular to the substrate asymmetry direction. At $qB/\alpha_d = 0.4$ in Fig. 8(a), there are strong oscillations in y but the oscillations are symmetric so $\langle V_y \rangle = 0$. There are much smaller oscillations in x but these oscillations are also symmetric and $\langle V_x \rangle = 0$. In Fig. 8(b) at $qB/\alpha_d = 1.2$, there are strong spikes in V_x in the positive x direction corresponding to net motion of the particles in this direction. Both positive and negative velocity spikes appear in V_y , but the spikes are stronger in the negative y direction, leading to ratcheting motion along $-y$. Figure 8(c) shows that at $qB/\alpha_d = 4.0$, there are velocity oscillations in both directions but $\langle V_x \rangle$ and $\langle V_y \rangle$ are both zero.

4. Ratchet Effects for Varied ac drives

In Fig. 9(a) we plot $\langle V_x \rangle$ and $\langle V_y \rangle$ versus F_{AC} for the system in Fig. 6 at $A_p = 0.75$ and $qB/\alpha_d = 1.2$ for driving parallel to the substrate asymmetry direction. Here, the velocities are zero for $F_{AC} < 0.6$ because the ac drive is not large enough to permit the particles to jump out of the wells. For $0.6 \leq F_{AC} < 1.8$, there is a strong ratchet effect where the particles move in the positive x and negative y directions, giving $\theta_H \approx 55^\circ$. We find a series of regions where the ratchet effect drops to zero, corresponding to ac drive amplitudes where the particle orbits become trapped inside the pinning troughs. In other regions, the ratchet effect is reduced but there is still finite ratcheting

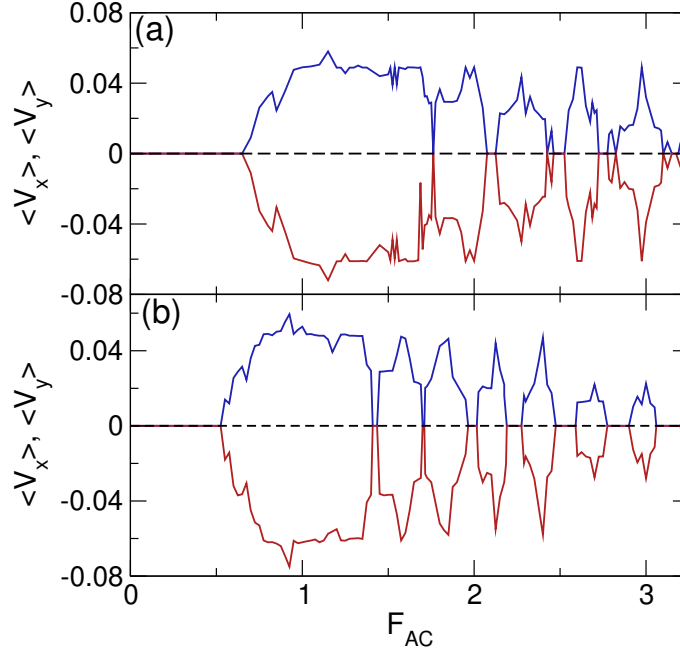


Figure 9. (a) $\langle V_x \rangle$ (blue) and $\langle V_y \rangle$ (red) vs F_{AC} for the system from Fig. 6 with $\rho = 0.208$ and $F_{AC} = 1.0$ at $A_p = 0.75$ and $qB/\alpha_d = 1.2$ for driving along x , parallel to the substrate asymmetry direction. (b) The same for driving along y , perpendicular to the substrate asymmetry direction. In both cases, there are regions where the ratchet efficiency drops to zero.

motion corresponding to orbits in which the particles move one lattice constant every other ac cycle or every n th ac cycle. For ac driving applied perpendicular to the substrate asymmetry direction, Fig. 9(b) shows a similar pattern of regions of reduced or zero ratcheting; however, the F_{AC} values at which zero velocities appear are shifted relative to the parallel driving case since the particle orbits are more tilted under perpendicular driving. Behavior similar to that shown in Fig. 9, with oscillations in the ratchet effectiveness as a function of ac amplitude, was observed previously in purely overdamped systems such as superconducting vortices on asymmetric 1D substrates [11]. In general, we find that the oscillations in ratchet efficiency are the most pronounced for low particle densities. At higher densities, oscillations appear for fillings at which the system is relatively ordered, while for incommensurate fillings, regions where the ratchet effect drops to zero are replaced with regions of finite but reduced ratchet effect.

In Fig. 10(a), we illustrate the particle locations and trajectories for the system in Fig. 9(b) for driving along y , perpendicular to the substrate asymmetry direction, at $F_{AC} = 0.5$ where the ratchet effect is zero. In this case, the particles oscillate in closed orbits, and there is no hopping from one well to the next. Figure 10(b) shows the trajectory of a single representative particle at $F_{AC} = 1.41$ where $\langle V_x \rangle = \langle V_y \rangle = 0$. Here each particle moves in a closed orbit spanning three pinning potential minima. At $F_{AC} = 1.6$, plotted in Fig. 10(c), there is a finite ratchet effect. Here, each particle follows a ratcheting trajectory that covers close to 3.5 pinning troughs per orbit. In Fig. 10(d) at $F_{AC} = 1.7$, the particles form closed orbits, and Fig. 9(b) indicates that there is zero ratchet effect. In this case, each particle circulates among four pinning minima. The ratchet effect

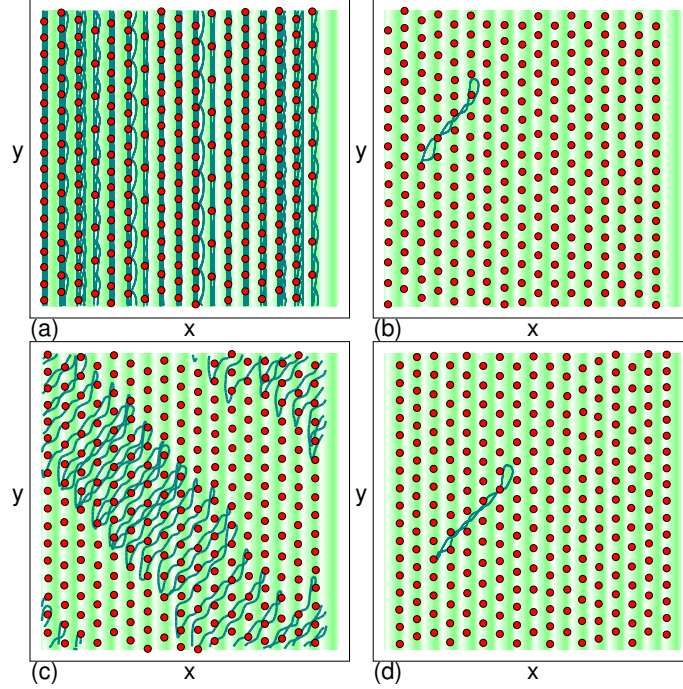


Figure 10. (a) Particle locations (red circles), substrate (green shading), and the trajectories of all the particles (lines) for the system in Fig. 9(b) with $\rho = 0.208$, $A_p = 0.75$, and $qB/\alpha_d = 1.2$ for driving along y , perpendicular to the substrate asymmetry direction, at $F_{AC} = 0.5$ where there is no ratchet effect. (b,c,d) The same but with the trajectory of only a single representative particle shown. (b) $F_{AC} = 1.41$, where there is no ratchet effect and the particle orbit is localized. (c) $F_{AC} = 1.6$, where there is a finite ratchet effect. (d) $F_{AC} = 1.7$, where the ratchet effect is absent and the particle motion is localized.

is generally lost in orbits where the particles are confined between n pinning minima, while there is a finite ratchet effect for incommensurate orbits. For driving along x , parallel to the substrate asymmetry direction, a similar trapping effect occurs for regions where the ratchet effect is zero; however, the particle orbits are more one-dimensional in character compared to the perpendicular driving case.

4.1. Ratchet Reversals for Varied Filling and Substrate Strength

We next consider the effect of varying the charge density ρ . In Fig. 11(a) we plot $\langle V_x \rangle$ and $\langle V_y \rangle$ versus ρ for a system with $A_p = 1.25$, $qB/\alpha_d = 1.2$, and $F_{AC} = 1.5$ for driving perpendicular to the substrate asymmetry direction. For $\rho < 1.0$, we find a ratchet effect in which the particles move in the positive x and negative y directions. This ratchet motion passes through a local maximum near $\rho = 0.5$. There is a reversal in the ratchet for $\rho > 1.0$, where the particles move in the positive y and negative x directions. Figure 11(b) shows the absolute value of the velocity $|\langle V \rangle|$ versus ρ , which peaks near $\rho = 0.5$ and has a drop near $\rho = 1.0$ at the point where the ratchet reversal occurs. In

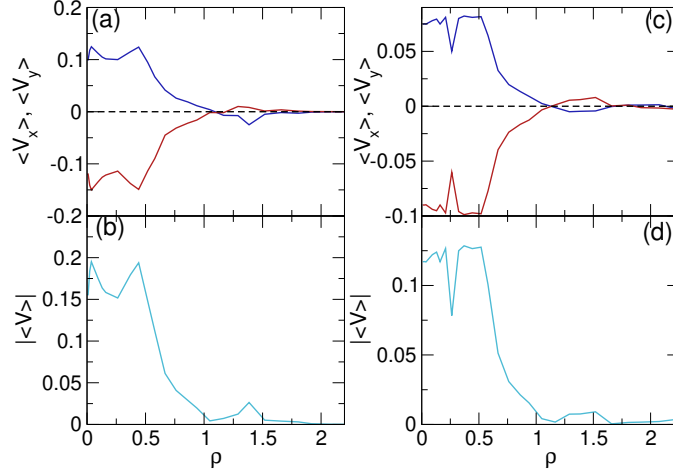


Figure 11. (a) $\langle V_x \rangle$ (blue) and $\langle V_y \rangle$ (red) vs particle density ρ for a system with $qB/\alpha_d = 1.2$, $A_p = 1.25$, and $F_{AC} = 1.5$ for driving along x , parallel to the substrate asymmetry direction. (b) The corresponding $|\langle V \rangle|$ vs ρ . (c) $\langle V_x \rangle$ (blue) and $\langle V_y \rangle$ (red) vs ρ for the same system but for driving along y , perpendicular to the substrate asymmetry direction. (d) The corresponding $|\langle V \rangle|$ vs ρ . There is a reversal in the ratchet effect as a function of increasing ρ for both ac driving directions.

the reversed ratchet regime, the absolute value of the velocity is much lower since the motion is produced by a small number of solitons in the lattice that can hop over the substrate barriers in the hard direction. During the $+x$ portion of the ac drive cycle, the particles form a more spread out configuration and the solitons are less well defined. In previous work performed at $qB/\alpha_d = 0.0$, a reversal of the ratchet effect was also observed as a function of increasing filling [36]. In Fig. 11(c), we plot $\langle V_x \rangle$ and $\langle V_y \rangle$ versus ρ for the same system from Fig. 11(a) but with the ac driving applied perpendicular to the substrate asymmetry direction. For $\rho < 1.0$, the motion is in the positive x and negative y directions. In the corresponding plot of $|\langle V \rangle|$ versus ρ in Fig. 11(d), there is a dip near $\rho = 0.25$ due to the formation of a commensurate lattice, which is better pinned by the substrate. For $\rho > 1.0$, the overall velocity is strongly reduced, and there is a ratchet reversal at $\rho \approx 1.2$ where the motion is in the positive y and negative x directions.

The magnitude and direction of the ratchet motion depends on both the filling fraction and the substrate strength. For lower fillings of $\rho < 0.77$, the ratchet motion is generally in the positive x direction; however, for higher fillings, the ratchet motion can be in either the positive or negative x direction. In Fig. 12(a) we plot $\langle V_x \rangle$ and $\langle V_y \rangle$ versus F_p for a system with $\rho = 0.938$, $F_{AC} = 1.0$, and $qB/\alpha_d = 1.2$ under driving along y , perpendicular to the substrate asymmetry, while Fig. 12(b) shows the corresponding $|\langle V \rangle|$ versus F_p . For $F_p < 0.6$ there is no ratchet effect. A positive ratchet effect with motion in the positive x and negative y directions appears for $0.6 \leq F_p < 1.3$, and is followed by a ratchet reversal for $1.3 \leq F_p < 3.0$, where the motion is in the positive y and negative x direction. When the ratchet reverses, the particle motion reverses direction. All of the particles are pinned for $F_p \geq 3.0$. Both the forward and reverse ratchet effects pass through peak efficiencies, leading to the appearance of a double peak feature in $|\langle V \rangle|$. Figure 12(c,d) shows $\langle V_x \rangle$, $\langle V_y \rangle$, and $|\langle V \rangle|$ versus F_p for the same system at a higher density of $\rho = 1.27$, where only a reversed ratchet effect occurs.

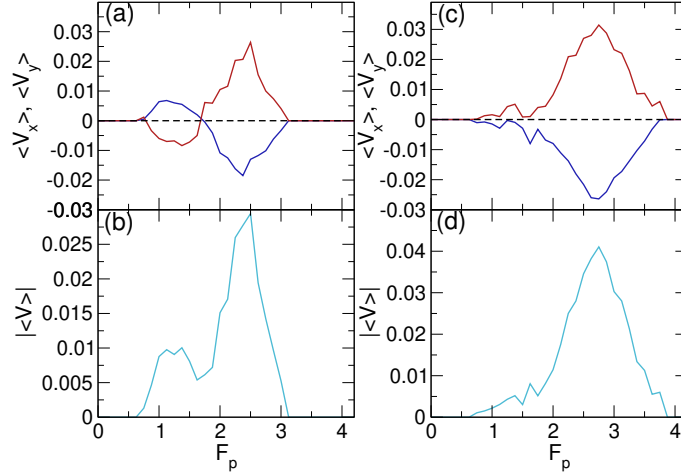


Figure 12. (a) $\langle V_x \rangle$ (blue) and $\langle V_y \rangle$ (red) vs F_p for a sample with $F_{AC} = 1.0$ and $qB/\alpha_d = 1.2$ for driving along y , perpendicular to the substrate asymmetry direction, at $\rho = 0.938$ where a ratchet reversal occurs. (b) The corresponding $|\langle V \rangle|$ vs F_p . (c) $\langle V_x \rangle$ (blue) and $\langle V_y \rangle$ (red) for the same system at $\rho = 1.27$ where there is only a reversed ratchet effect. (d) The corresponding $|\langle V \rangle|$ vs F_p .

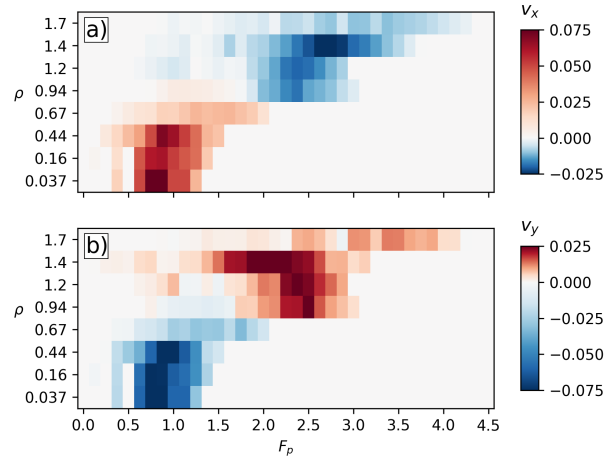


Figure 13. Heat map of the ratchet velocity as a function of ρ vs F_p for the system in Fig. 12 with $F_{AC} = 1.0$ and $qB/\alpha_d = 1.2$ for driving along y , perpendicular to the substrate asymmetry direction. (a) $\langle V_x \rangle$. (b) $\langle V_y \rangle$. The change in color from red tones to blue tones (or vice versa) indicates a ratchet reversal.

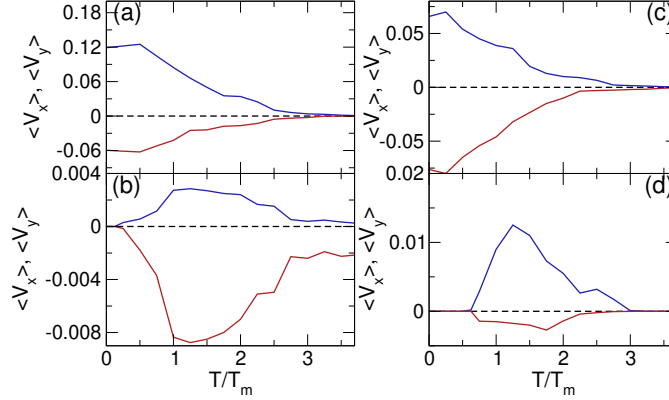


Figure 14. $\langle V_x \rangle$ (blue) and $\langle V_y \rangle$ (red) vs temperature T/T_m in samples with $A_p = 0.75$, $\rho = 0.208$, and $F_{AC} = 1.0$. Here T_m is the temperature at which the substrate-free system thermally melts. (a,b) x direction ac driving parallel to the substrate asymmetry direction at (a) $qB/\alpha_d = 0.5$ and (b) $qB/\alpha_d = 3.0$. (c,d) y direction ac driving perpendicular to the substrate asymmetry direction at (c) $qB/\alpha_d = 1.0$ and (d) $qB/\alpha_d = 0.4$.

In Fig. 13(a,b), we plot heat maps of $\langle V_x \rangle$ and $\langle V_y \rangle$ as a function of ρ versus F_p for the system from Fig. 12, highlighting both the forward and reverse ratchet effects. For $\rho < 0.83$, the ratchet motion is primarily in the positive x and negative y directions, with a reversal in the ratchet motion occurring at high densities. It is possible that additional ratchet reversals could occur for higher values of ρ than those considered in this work.

5. Thermal Effects

We next consider the effect of adding thermal Langevin kicks to the particle motion in order to represent a finite temperature. We use a system with $A_p = 0.75$, $\rho = 0.208$, and $F_{AC} = 1.0$, and we report temperature in terms of T/T_m , where T_m is the temperature at which the substrate-free system thermally disorders. In Fig. 14(a) we plot $\langle V_x \rangle$ and $\langle V_y \rangle$ versus T/T_m at $qB/\alpha_d = 0.5$ for driving parallel to the substrate asymmetry direction. There is initially a slight increase in the ratchet effect with increasing T/T_m followed by a pronounced drop in ratchet motion for $T/T_m > 1.0$. The decrease occurs since the thermal fluctuations reduce the effectiveness of the substrate, and for $T/T_m > 1.0$, thermal hopping is strongly enhanced. Figure 14(b) shows $\langle V_x \rangle$ and $\langle V_y \rangle$ versus T/T_m for the same system at $qB/\alpha_d = 3.0$, where for $T/T_m = 0$, the magnetic field is large enough to localize the motion and prevent ratchet motion from occurring. In this case, we find that the ratcheting motion reaches a maximum for $T/T_m > 1.0$ and then diminishes; however, the maximum velocity of the ratchet motion is considerably reduced compared to that found at the lower value of qB/α_d . In Fig. 14(c) we illustrate $\langle V_x \rangle$ and $\langle V_y \rangle$ versus T/T_m for the same system at $qB/\alpha_d = 1.0$ but for driving perpendicular to the substrate asymmetry direction. Here the ratchet effect generally decreases with increasing T/T_m . At $qB/\alpha_d = 0.4$ in the same system, shown in Fig. 14(d), no ratchet motion occurs when $T/T_m = 0$; however, for $T/T_m > 1.0$, thermal hopping of the particles out of the substrate troughs produces a ratchet effect that is gradually destroyed at

high temperatures. For $qB/\alpha_d > 3.0$, driving perpendicular to the substrate asymmetry and driving parallel to the substrate both produce similar behavior in which there is finite ratchet motion that appears for $T/T_m > 1.0$ and then diminishes with increasing temperature. These results show that even for systems with strong thermal effects or in a Wigner liquid, the transverse ratchet effects should be robust.

6. Summary

We have examined ratchet effects for a two-dimensional system of charged particles in a magnetic field interacting with a one dimensional asymmetric substrate under ac driving applied either parallel or perpendicular to the substrate asymmetry direction. When the magnetic field is zero, a ratchet effect only occurs when the ac drive is parallel to the substrate asymmetry direction. Under a finite magnetic field, however, a transverse ratchet effect can occur in which the particles move both parallel and perpendicular to the substrate asymmetry direction due to the finite Hall angle produced by the cyclotron motion of the particles. When the ac drive is applied perpendicular to the substrate asymmetry direction, a transverse ratchet effect can occur. For fixed ac driving amplitude, the ratchet effect drops to zero at higher fields when the charge motion becomes localized inside the pinning troughs. We have investigated this ratchet effect for varied magnetic fields, substrate strengths, ac drive amplitudes, and charge density. We find that there can be reversals of the ratchet effect at higher charge densities, where the particles move against the easy flow direction of the substrate asymmetry. The reversed ratchet motion can occur for driving either parallel or perpendicular to the substrate asymmetry direction. Our results demonstrate that cyclotron motion and the resulting finite Hall angle can produce new kinds of ratchet effects that could be relevant for Wigner crystals, charged colloids, dusty plasmas, and other charged systems coupled to an asymmetric substrate in the presence of a magnetic field.

Acknowledgements

We gratefully acknowledge the support of the U.S. Department of Energy through the LANL/LDRD program for this work. This work was supported by the US Department of Energy through the Los Alamos National Laboratory. Los Alamos National Laboratory is operated by Triad National Security, LLC, for the National Nuclear Security Administration of the U. S. Department of Energy (Contract No. 892333218NCA000001).

References

- [1] Magnasco M O 1993 *Phys. Rev. Lett.* **71**(10) 1477–1481
- [2] Astumian R D and Bier M 1994 *Phys. Rev. Lett.* **72**(11) 1766–1769
- [3] Reimann P 2002 *Phys. Rep.* **361** 57–265
- [4] Rousselet J, Salome L, Ajdari A and Prost J 1994 *Nature (London)* **370** 446–448
- [5] Marquet C, Buguin A, Talini L and Silberzan P 2002 *Phys. Rev. Lett.* **88**(16) 168301
- [6] Lau B, Kedem O, Schwabacher J, Kwasniewski D and Weiss E A 2017 *Mater. Horiz.* **3** 310–318
- [7] Reichhardt C J O and Reichhardt C 2017 *Ann. Rev. Condens. Matter Phys.* **8** 51–75
- [8] Farkas Z, Szalai F, Wolf D E and Vicsek T 2002 *Phys. Rev. E* **65**(2) 022301
- [9] Mennerat-Robilliard C, Lucas D, Guibal S, Tabosa J, Jurczak C, Courtois J Y and Grynberg G 1999 *Phys. Rev. Lett.* **82**(4) 851–854
- [10] Lundh E and Wallin M 2005 *Phys. Rev. Lett.* **94**(11) 110603
- [11] Lee C S, Jankó B, Derényi I and Barabási A L 1999 *Nature (London)* **400** 337–340
- [12] Wambaugh J F, Reichhardt C, Olson C J, Marchesoni F and Nori F 1999 *Phys. Rev. Lett.* **83**(24) 5106–5109

- [13] Salger T, Kling S, Hecking T, Geckeler C, Morales-Molina L and Weitz M 2009 *Science* **326** 1241–1243
- [14] Derényi I and Vicsek T 1995 *Phys. Rev. Lett.* **75**(3) 374–377
- [15] McDermott D, Olson Reichhardt C J and Reichhardt C 2016 *Soft Matter* **12**(41) 8606–8615
- [16] Villegas J E, Savel'ev S, Nori F, Gonzalez E M, Anguita J V, García R and Vicent J L 2003 *Science* **302** 1188–1191
- [17] de Souza Silva C C, de Vondel J V, Morelle M and Moshchalkov V V 2006 *Nature (London)* **440** 651–654
- [18] Dinis L, González E M, Anguita J V, Parrondo J M R and Vicent J L 2007 *Phys. Rev. B* **76**(21) 212507
- [19] Lu Q, Reichhardt C J O and Reichhardt C 2007 *Phys. Rev. B* **75**(5) 054502
- [20] Yu K, Heitmann T W, Song C, DeFeo M P, Plourde B L T, Hesselberth M B S and Kes P H 2007 *Phys. Rev. B* **76**(22) 220507
- [21] Gillijns W, Silhanek A V, Moshchalkov V V, Reichhardt C J O and Reichhardt C 2007 *Phys. Rev. Lett.* **99**(24) 247002
- [22] Lin N S, Heitmann T W, Yu K, Plourde B L T and Misko V R 2011 *Phys. Rev. B* **84**(14) 144511
- [23] Van de Vondel J, Gladilin V N, Silhanek A V, Gillijns W, Tempere J, Devreese J T and Moshchalkov V V 2011 *Phys. Rev. Lett.* **106**(13) 137003
- [24] Shklovskij V A, Sosedkin V V and Dobrovolskiy O V 2014 *J. Phys.: Condens. Matter* **26** 025703
- [25] Reichhardt C, Ray D and Reichhardt C J O 2015 *Phys. Rev. B* **91**(18) 184502
- [26] Dobrovolskiy O, Begun E, Bezv V, Sachser R and Huth M 2020 *Phys. Rev. Applied* **13**(2) 024012
- [27] Lyu Y Y, Jiang J, Wang Y L, Xiao Z L, Dong S, Chen Q H, Milosevic M V, Wang H, Divan R, Pearson J E, Wu P, Peeters F M and Kwok W K 2021 *Nature Commun.* **12** 2703
- [28] Tierno P and Fischer T M 2014 *Phys. Rev. Lett.* **112**(4) 048302
- [29] Wigner E 1934 *Phys. Rev.* **46**(11) 1002–1011
- [30] Monceau P 2012 *Adv. Phys.* **61** 325–581
- [31] Falson J, Sodemann I, Skinner B, Tabrea D, Kozuka Y, Tsukazaki A, Kawasaki M, von Klitzing K and Smet J H 2022 *Nature Mater.* **21** 311–316
- [32] Shayegan M 2022 *Nature Rev. Phys.* **4** 212–213
- [33] Russell E R, Spaepen F and Weitz D A 2015 *Phys. Rev. E* **91**(3) 032310
- [34] Schmidt J, Lambrecht A, Weckesser P, Debatin M, Karpa L and Schaetz T 2018 *Phys. Rev. X* **8**(2) 021028
- [35] Li W, Huang D, Reichhardt C, Reichhardt C J O and Feng Y 2023 *Phys. Rev. Res.* **5**(2) 023008
- [36] Reichhardt C and Reichhardt C J O 2023 *Phys. Rev. B* in press
- [37] Brown L S, Gabrielse G, Helmerson K and Tan J 1985 *Phys. Rev. A* **32**(6) 3204–3218
- [38] Müller J E 1992 *Phys. Rev. Lett.* **68**(3) 385–388
- [39] Weiss D, Roukes M L, Menschig A, Grambow P, von Klitzing K and Weimann G 1991 *Phys. Rev. Lett.* **66** 2790–2793
- [40] Weiss D, Richter K, Menschig A, Bergmann R, Schweizer H, von Klitzing K and Weimann G 1993 *Phys. Rev. Lett.* **70**(26) 4118–4121
- [41] Wiersig J and Ahn K H 2001 *Phys. Rev. Lett.* **87**(2) 026803
- [42] Khoury M, Lacasta A M, Sancho J M, Romero A H and Lindenberg K 2008 *Phys. Rev. B* **78**(15) 155433
- [43] Reichhardt C and Reichhardt C J O 2021 *Phys. Rev. B* **103**(12) 125107
- [44] Nagaosa N and Tokura Y 2013 *Nature Nanotechnol.* **8** 899–911
- [45] Reichhardt C, Reichhardt C J O and Milosevic M 2022 *Rev. Mod. Phys.* **94** 035005
- [46] Schulz T, Ritz R, Bauer A, Halder M, Wagner M, Franz C, Pfeleiderer C, Everschor K, Garst M and Rosch A 2012 *Nature Phys.* **8** 301–304
- [47] Ma X, Reichhardt C J O and Reichhardt C 2017 *Phys. Rev. B* **95**(10) 104401
- [48] Göbel B and Mertig I 2021 *Sci. Rep.* **11** 3020
- [49] Reichhardt C and Reichhardt C J O 2022 *Phys. Rev. B* **106**(23) 235417
- [50] Reichhardt C, Ray D and Reichhardt C J O 2015 *New J. Phys.* **17** 073034
- [51] Chen W, Liu L and Zheng Y 2020 *Phys. Rev. Applied* **14**(6) 064014
- [52] Ai B 2016 *Sci. Rep.* **6** 18740
- [53] Liu G, Rumyantsev S, Bloodgood M A, Salguero T T and Balandin A A 2018 *Nano Lett.* **18**(6) 3630–3636
- [54] Crandall R S and Williams R 1971 *Phys. Lett. A* **34** 404–405
- [55] Grimes C C and Adams G 1979 *Phys. Rev. Lett.* **42**(12) 795–798
- [56] Doman B G S 1979 *J. Phys. C: Solid State Phys.* **12** 3757–3760
- [57] Bello M S, Levin E I, Shklovskii B I and Efros A L 1981 *Zh. Eksp. Teor. Fiz.* **80** 1596–1612 [*Sov. Phys. JETP* **53**(4), 822–829 (1981)]
- [58] Dykman M I 1980 *Solid State Commun.* **35** 753–757
- [59] Andrei E Y, Deville G, Glatli D C, Williams F I B, Paris E and Etienne B 1988 *Phys. Rev. Lett.* **60**(26) 2765–2768

- [60] Goldman V J, Santos M, Shayegan M and Cunningham J E 1990 *Phys. Rev. Lett.* **65**(17) 2189–2192
- [61] Jiang H W, Stormer H L, Tsui D C, Pfeiffer L N and West K W 1991 *Phys. Rev. B* **44**(15) 8107–8114
- [62] Williams F I B, Wright P A, Clark R G, Andrei E Y, Deville G, Glattli D C, Probst O, Etienne B, Dorin C, Foxon C T and Harris J J 1991 *Phys. Rev. Lett.* **66**(25) 3285–3288
- [63] Kopelevich Y, da Silva R R, Rougier A and Luk'yanchuk I A 2007 *Phys. Lett. A* **368** 419–422
- [64] Brussarski P, Li S, Kravchenko S V, Shashkin A A and Sarachik M P 2018 *Nature Commun.* **9** 3803
- [65] Hossain M S, Ma M K, Villegas-Rosales K A, Chung Y J, Pfeiffer L N, West K W, Baldwin K W and Shayegan M 2022 *Phys. Rev. Lett.* **129**(3) 036601
- [66] Shirahama K and Kono K 1995 *Phys. Rev. Lett.* **74**(5) 781–784
- [67] Piacente G and Peeters F M 2005 *Phys. Rev. B* **72**(20) 205208
- [68] Araki M and Hayakawa H 2012 *Phys. Rev. B* **86** 165412
- [69] Rees D G, Totsuji H and Kono K 2012 *Phys. Rev. Lett.* **108**(17) 176801
- [70] Rees D G, Beysengulov N R, Lin J J and Kono K 2016 *Phys. Rev. Lett.* **116**(20) 206801
- [71] Moskovtsev K and Dykman M I 2020 *Phys. Rev. B* **101**(24) 245435
- [72] Regan E C, Wang D, Jin C, Utama M I B, Gao B, Wei X, Zhao S, Zhao W, Zhang Z, Ymigeta K, Blei M, Carlström J D, Watanabe K, Taniguchi T, Tongay S, Crommie M, Zettl A and Wang F 2020 *Nature* **579** 359–363
- [73] Xu Y, Liu S, Rhodes D A, Watanabe K, Taniguchi T, Hone J, Elser V, Mak K F and Shan J 2020 *Nature (London)* **587** 214–218
- [74] Huang X, Wang T, Miao S, Wang C, Li Z, Lian Z, Taniguchi T, Watanabe K, Okamoto S, Xiao D, Shi S F and Cui Y T 2021 *Nature Phys.* **17** 715–719
- [75] Li H, Li S, Regan E C, Wang D, Zhao W, Kahn S, Yumigeta K, Blei M, Taniguchi T, Watanabe K, Tongay S, Zettl A, Crommie M F and Wang F 2021 *Nature (London)* **597** 650–654
- [76] Matty M and Kim E A 2022 *Nature Commun.* **13** 7098
- [77] Mak K F and Shan J 2022 *Nature Nanotechnol.* **17** 686–695
- [78] Chen G, Zhang Y H, Sharpe A, Zhang Z, Wang S, Jiang L, Lyu B, Li H, Watanabe K, Taniguchi T, Shi Z, Goldhaber-Gordon D, Zhang Y and Wang F 2023 *Nano Lett.* **23** 7023–7028
- [79] Smoleński T, Dolgirev P E, Kühlenkamp C, Popert A, Shimazaki Y, Back P, Lu X, Kroner M, Watanabe K, Taniguchi T, Esterlis I, Demler E and Imamoglu A 2021 *Nature (London)* **595** 53–57
- [80] Cha M C and Fertig H A 1994 *Phys. Rev. Lett.* **73**(6) 870–873
- [81] Reichhardt C, Olson C J, Grønbech-Jensen N and Nori F 2001 *Phys. Rev. Lett.* **86**(19) 4354–4357
- [82] Csáthy G A, Tsui D C, Pfeiffer L N and West K W 2007 *Phys. Rev. Lett.* **98**(6) 066805
- [83] Zakharov M Y, Demidov D and Shepelyansky D L 2019 *Phys. Rev. B* **99**(15) 155416
- [84] He Y, Ai B, Dai C, Song C, Wang R, Sun W, Liu F and Feng Y 2020 *Phys. Rev. Lett.* **124**(7) 075001
- [85] Reichhardt C and Reichhardt C J O 2020 *Phys. Rev. E* **101**(6) 062602
- [86] Lekner J 1991 *Physica A* **176** 485–498
- [87] Grønbech-Jensen N 1997 *Int. J. Mod. Phys. C* **8** 1287–1297